IOPscience iopscience.iop.org

Home Search Collections Journals About Contact us My IOPscience

Single-particle dynamics in dense granular fluids under driving

This article has been downloaded from IOPscience. Please scroll down to see the full text article.

2012 EPL 98 28001

(http://iopscience.iop.org/0295-5075/98/2/28001)

View the table of contents for this issue, or go to the journal homepage for more

Download details:
IP Address: 134.76.88.80
The article was downloaded on 30/04/2013 at 15:19

Please note that terms and conditions apply.

epl A Letters Journal Exploring the Frontiers of Physics

April 2012

EPL, **98** (2012) 28001 www.epljournal.org
doi: 10.1209/0295-5075/98/28001

Single-particle dynamics in dense granular fluids under driving

Matthias Sperl[1(a)], W. Till Kranz[2,3] and Annette Zippelius[2,3]

[1] *Institut für Materialphysik im Weltraum, Deutsches Zentrum für Luft- und Raumfahrt (DLR) 51170 Köln, Germany, EU*
[2] *Max-Planck-Institut für Dynamik und Selbstorganisation - Am Fassberg 17, 37077 Göttingen, Germany, EU*
[3] *Georg-August-Universität Göttingen, Institut für Theoretische Physik - Friedrich-Hund-Platz 1, 37077 Göttingen, Germany, EU*

received 24 January 2012; accepted in final form 19 March 2012
published online 24 April 2012

PACS 81.05.Rm – Porous materials; granular materials
PACS 61.20.Lc – Time-dependent properties; relaxation
PACS 64.70.P- – Glass transitions of specific systems

Abstract – We present a mode-coupling theory for the dynamics of a tagged particle in a driven granular fluid close to the glass transition. The mean-squared displacement is shown to exhibit a plateau indicating structural arrest. In contrast to elastic hard-sphere fluids, which are solely controlled by volume fraction, the localisation length as well as the critical dynamics depend on the degree of dissipation, parametrized by the coefficient of normal restitution ε. Hence the resulting glassy structure as well as the critical dynamics are nonuniversal with respect to ε.

Copyright © EPLA, 2012

Introduction. – Experimental investigations [1–4] as well as simulations [5,6] of dense assemblies of agitated granular beads show signatures of a transition from fluid to glassy behavior. Motivated by the striking similarity between the measurements for granular systems —necessarily far from equilibrium — and for equilibrium colloidal systems, we have recently generalized the mode-coupling theory of the coherent density autocorrelation function $\phi_q(t)$ to driven dissipative systems [7]. Here, we extend the analysis to the single-particle dynamics and compute the incoherent density autocorrelation function $\phi_q^s(t)$ as well as the mean-squared displacement (MSD), which are directly accessible to experiments.

In two dimensions, experimental measurements of the MSD $\delta r^2(t)$ are available by direct imaging from air fluidized [3] and mechanically agitated systems [4]. In three dimensions, the MSD is observed by diffusive-wave spectroscopy (DWS) in gravity-driven flows of glass beads in ambient air [1] and in a water-fluidized bed [2]. All these studies as well as computer simulations [6] in two-dimensional systems reveal the development of a plateau in the MSD and relate their findings to glassy dynamics. With analogous results from colloidal dispersions in mind, this has been interpreted as the signature of a granular glass transition. Measurements of additional observables support this interpretation. Namely, the incoherent scattering function has been found to develop a two-step relaxation at high densities both in experiments [4] and in simulations [6]. Moreover, plateaus extending over increasingly larger windows in time imply a strong decrease of the diffusion coefficient $D = \lim_{t\to\infty}\delta r^2(t)/6t$ [3,5,6] accompanied by a strong increase of relaxation times, τ, [4,6] upon approaching the granular glass transition density.

For systems in thermal equilibrium, mode-coupling theory (MCT) has become an established tool for the investigation of glassy dynamics, it describes many experimental features and has the potential for nontrivial predictions [8]. Applied to the case of colloidal suspensions, it is found that MCT is quantitatively accurate to about 20% in the density. For the mean-squared displacement, MCT describes the measured data for the entire regime available which is over eight orders of magnitude in time [9,10].

The granular mode-coupling theory for homogeneously driven systems, outlined in ref. [7], predicts 1) the existence of a glass transition, *i.e.*, $\lim_{t\to\infty}\phi_q(t) = f_q > 0$, 2) an increase of the packing fraction at the transition, $\varphi^c(\varepsilon)$, with increased dissipation quantified by the normal coefficient of restitution ε, and 3) changes to the dynamical exponents with dissipation.

While the glass transition within MCT is found to be a singularity in the coherent functions $\phi_q(t)$, incoherent scattering functions $\phi_q^s(t)$ and in particular the MSD, $\delta r^2(t)$, have been measured in the experiments and simulations discussed above. In order to compare to such data,

(a) E-mail: matthias.sperl@dlr.de

the MCT for incoherent functions is derived for granular systems in the following.

Model. – We consider a granular fluid consisting of N hard spheres of mass $m=1$ and diameter d in a volume V. Particle positions and velocities are denoted by $\{\vec{r}_i, \vec{v}_i\}$ and we will consider the thermodynamic limit such that the density $n=N/V$ is finite. Energy dissipation in binary collisions is modeled by incomplete normal restitution, quantified by a constant coefficient of restitution ε. To achieve a stationary state the system is driven randomly and homogeneously: All particles are kicked stochastically at random time intervals. This allows the system to relax to a stationary state with finite temperature, T, defined as the average kinetic energy of the particles.

It is important to note that the system is not in equilibrium so that the N-particle distribution function, $w(\Gamma)$, is in general unknown. We assume [11] that positions and velocities are uncorrelated, $w(\Gamma)=w_r(\{\vec{r}_i\})w_v(\{\vec{v}_i\})$, and that the velocity distribution factorizes into a product of one-particle distributions, $w_v(\{\vec{v}_i\})=\prod_i w_1(\vec{v}_i)$. The precise from of $w_1(\vec{v})$ is not needed, it only has to satisfy $\frac{1}{N}\sum_i \vec{v}_i^{\,2}=3T$, finite. Furthermore, the system is assumed to be isotropic and homogeneous except for the excluded volume interaction: $w_r(\{\vec{r}_i\})=\prod_{i<j}\theta(r_{ij}-d)$.

Granular mode-coupling theory. – The dynamics can be formulated in terms of a Pseudo-Liouville operator [12], so that techniques for the derivation of MCT for energy-conserving systems with Newtonian dynamics in [13] can be used with appropriate changes [7]. The central quantity to describe the dynamics of a tagged particle is the incoherent intermediate scattering function

$$\phi_q^s(t) := \left[\int \mathrm{d}\Gamma w(\Gamma)\frac{1}{N}\sum_i \exp(i\vec{q}\cdot(\vec{r}_i(t)-\vec{r}_i(0))\right],$$

where $[\ldots]$ denotes the average over the random driving.

Using appropriate Mori-projectors, one finds that $\phi_q^s(t)$ obeys the following equation of motion:

$$\begin{aligned}&\partial_t^2\phi_q^s(t)+\nu_q^s\partial_t\phi_q^s(t)+\Omega_{s\,q}^2\phi_q^s(t)\\&+\Omega_{s\,q}^2\int_0^t \mathrm{d}t' m_q^s(t-t')\partial_{t'}\phi_q^s(t')=0,\end{aligned} \tag{1a}$$

formally identical to the equation of motion for an energy conserving system. Here the friction, ν_q^s, is given by the same expression as for the coherent part:

$$\nu_q^s=\nu_E\frac{1+\varepsilon}{2}[1-j_0(qd)+2j_2(qd)] \tag{1b}$$

with j_i the spherical Bessel functions and with the classical (equilibrium) Enskog collision rate $\nu_E=4\sqrt{\pi}nd^2g_dv_0$ [14] where g_d is the contact value of the pair distribution function $g(r)$ and $v_0=\sqrt{T/m}$ is the thermal velocity. Following ref. [7], we applied the mode-coupling approximation to the memory kernel $m_q^s(t)$,

$$m_q^s(t)\simeq\frac{1+\varepsilon}{2}\frac{n}{q^2}\int\frac{\mathrm{d}^3k}{(2\pi)^3}(\hat{\boldsymbol{q}}\cdot\boldsymbol{k})^2S_kc_k^2\phi_k(t)\phi_{|\boldsymbol{q}-\boldsymbol{k}|}^s(t). \tag{1c}$$

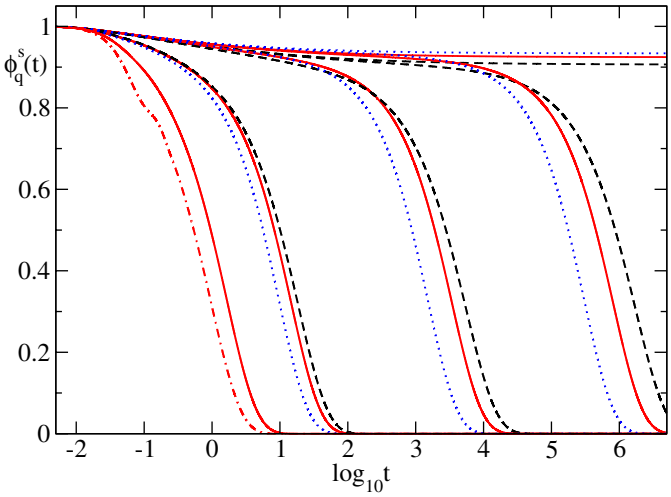

Fig. 1: (Colour on-line) Incoherent scattering functions $\phi_q^s(t)$ for coefficient of restitution $\varepsilon=1.0$ (dashed curve, elastic case), 0.5 (full curve), and 0.0 (dotted curve) for packing fractions φ from right to left: at the glass transition $\varphi^c(\varepsilon)$, and at $0.999\varphi^c(\varepsilon)$, $0.99\varphi^c(\varepsilon)$, and $0.9\varphi^c(\varepsilon)$, respectively. Solutions of eq. (1a) are presented for the wave vector $qd=4.2$. For $\varepsilon=0.5$, an additional solution is shown for $\varphi=0.4$ and accompanied with a solution where the damping ν_q is set to zero (chain line).

Details of the derivation from the microscopic dynamics will be published elsewhere. Here the $\phi_q(t)$ are given by the solutions of the coherent MCT equations [7], S_k denotes the static structure factor and c_k the direct correlation function. In contrast to the coherent case, the frequency $\Omega_{s\,q}^2=q^2T$ does not carry any dependence on the coefficient of restitution ε. The equations of motion, eq. (1), are solved with the initial conditions $\phi_q^s(0)=1, \partial_t\phi_q^s(0)=0$. The numerical algorithms for solving the equations of motion for the coherent and the incoherent intermediate scattering function as well as for the MSD have been introduced previously [7,10,15].

To be consistent with the results for the coherent functions [7], equilibrium values are used in the calculations for the static structure within the Percus-Yevick approximation [16]. This approximation can be relaxed by using directly the static structure from numerical simulation.

Intermediate scattering functions. – Figure 1 shows the solutions for the wave vector $qd=4.2$ which is at about half of the principal peak in the static structure factor S_q. For increasing packing fraction $\varphi=\pi nd^3/6$, the scattering functions develop a plateau for $0\leqslant\varepsilon\leqslant1$. For smaller ε, the critical plateau value $f_q^s=\lim_{t\to\infty}\phi_q^s(t)$ at the transition point increases. It is seen in fig. 2 that this increase with ε applies to all wave vectors for f_q^s. The increase results in a growing half width of f_q^s as a function of wave number, which is related to the inverse localization length of a tagged particle.

One important result of MCT is the existence of two time scales, which both diverge with the distance from

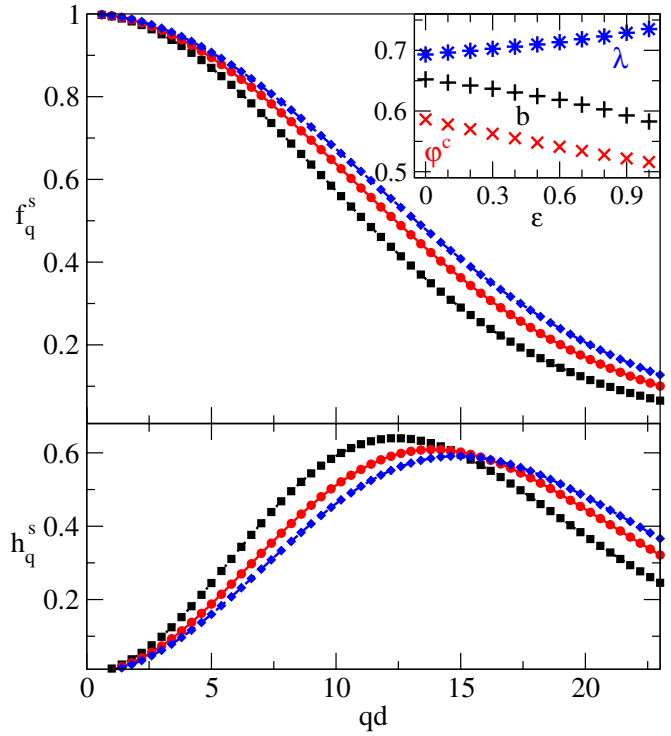

Fig. 2: (Colour on-line) Glass form factors f_q^s (upper panel) and critical amplitudes h_q^s (lower panel), cf. eq. (2), for the incoherent scattering functions for coefficient of restitution $\varepsilon =$ 1.0 (squares), 0.5 (circles), and 0.0 (diamonds). The inset shows the exponent parameter $\lambda(*)$, the von-Schweidler exponent $b(+)$, and the packing fraction at the transition φ^c $(\times)$ depending on the coefficient of restitution ε.

the critical point, $\sigma = (\varphi_c - \varphi)/\varphi_c$. The first one, $t_\sigma \propto \sigma^{-1/(2a)}$ rules the dynamics near the plateau, whereas $\tau \propto \sigma^{-\gamma}, \gamma = 1/(2a) + 1/(2b)$ determines the asymptotic time dependence, *i.e.*, the α-relaxation and the critical behavior of the diffusion coefficient. As for the elastic case, both exponents a and b are expressed by a single exponent parameter λ, which varies with ε as shown in the inset of fig. 2.

The plateau values, or glass form factors, f_q^s form the basis for the asymptotic expansion of the MCT equations of motion around the plateau [17]. Close to the transition point, the correlation function in the vicinity of the plateau can be expanded in leading order as

$$\phi_q^s(t;\sigma) = f_q^s + h_q^s G_\sigma(t), \tag{2a}$$

which defines the critical amplitudes h_q^s shown in the lower panel of fig. 2. While f_q^s and h_q^s are fixed by the details of the equations of motion at the transition point, $\sigma = 0$, the scaling function $G_\sigma(t)$ depends only on the time t and the distance σ from the transition point. The scaling law (2a) reveals a factorization property unique to glassy dynamics, where the complex dynamics can be separated into a time-dependent and a wave-number–dependent part. Directly

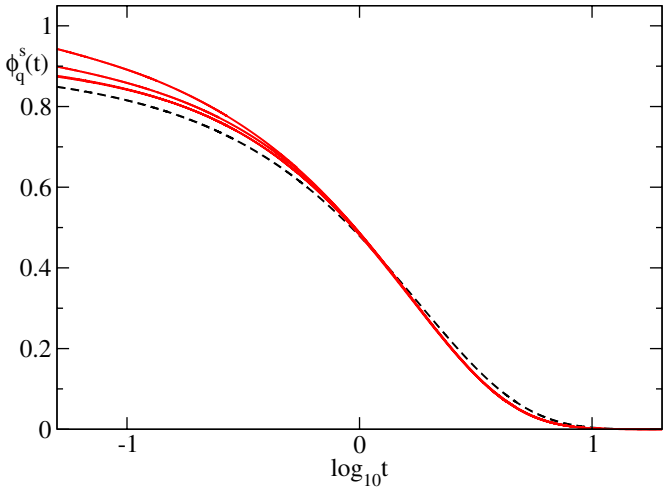

Fig. 3: (Colour on-line) α-scaling of the correlators of fig. 1 for coefficient of restitution $\varepsilon = 0.5$ (full curves). Curves are matched at $\phi_q^s(t) = 0.4$. For comparison, the curve for the elastic fluid at $0.999\varphi^c(\varepsilon)$ is shown as dashed line.

at the transition point, eq. (2a) reduces to the critical law

$$\phi_q^s(t;\sigma) = f_q^s + h_q^s (t/t_0)^{-a}, \tag{2b}$$

with a microscopic time scale t_0 and the exponent a which is shown in the inset of fig. 2 of [7]. In the fluid state, close to the transition, the above power law describes the approach to the plateau value. In the fluid state below the transition, $G_\sigma(t)$ describes the decay from the plateau to zero and in this regime is known as the von-Schweidler law

$$\phi_q^s(t;\sigma) = f_q^s - h_q^s (t/\tau)^b. \tag{2c}$$

For asymptotically long times, $t \gg t_\sigma$, the incoherent scattering functions obey the so-called α-scaling

$$\phi_q^s(t;\sigma) = \tilde{\phi}_q^s(t/\tau(\sigma)), \tag{3}$$

which connects to the von-Schweidler law for $x = t/\tau \leqslant 1$, whereas for large x, the decay is close to a Kohlrausch law [18], and crossing over to an exponential for the largest x. The scaling suggested by eq. (3) is applied to the results for $\varepsilon = 0.5$ from fig. 1 and displayed in fig. 3. Time scales τ are determined where the correlation functions cross the value $\tilde{\phi}_q^s(\tau) = 0.4$, and the curves are scaled on top of the first correlator accordingly. When getting closer to the transition, the correlation functions follow a master curve for progressively longer times. In contrast, an equally extended correlation function for the elastic case, *i.e.*, a different value for ε, clearly violates that scaling. With the form factors, f_q^s, and amplitudes, h_q^s, as well as the exponents b, all being nontrivial functions of ε no such scaling is expected.

The divergence of the time scale, τ, determines the vanishing of the diffusion constant D. Both singularities are governed by the asymptotic law $D \propto \tau^{-1} \propto \sigma^\gamma$ which is shown by full lines in fig. 4. Individual symbols in

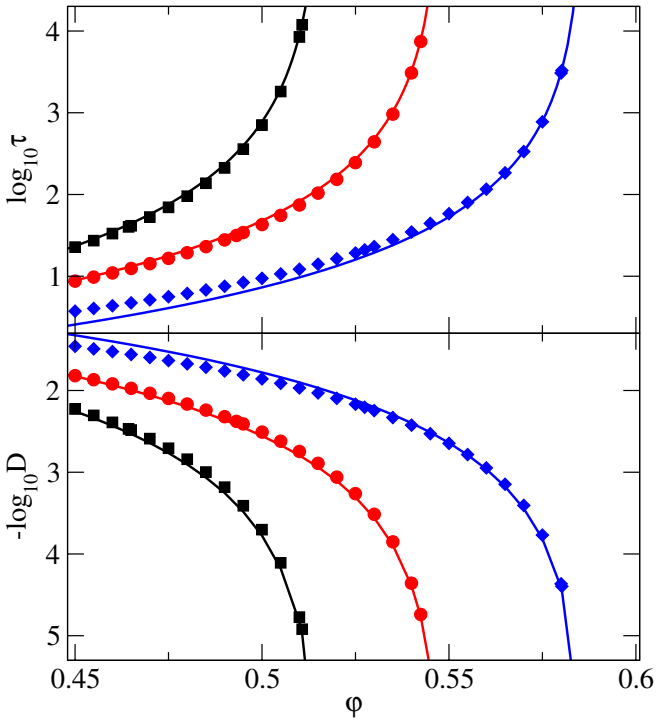

Fig. 4: (Colour on-line) Dependence on the packing fraction, φ, of the time scale τ where the incoherent scattering function $\phi_q^s(\tau) = 0.1$ (upper panel), and diffusion coefficients D (lower panel) derived from the numerical solutions of the equations of motion for coefficient of restitution $\varepsilon = 1.0$ (squares), 0.5 (circles), and 0.0 (diamonds). The full lines show the corresponding asymptotic laws $\tau \propto [\varphi^c(\varepsilon) - \varphi(\varepsilon)]^{-\gamma}$ and $D \propto [\varphi^c(\varepsilon) - \varphi(\varepsilon)]^{\gamma}$. For $\varepsilon = 1.0$, 0.5, and 0.0, the values for γ are 2.46239, 2.34921, and 2.28282, respectively.

the same plots show the actual values retrieved from the numerical solution of the equations of motion. The upper panel demonstrates that for sufficiently large time scales the asymptotic law describes the numerical values satisfactorily. On the contrary, for distances around 10% from the critical point and larger, one cannot expect the asymptotic law to hold —and the early part of the divergence might even suggest a power law with a different exponent.

The evolution of the diffusion coefficients in the lower panel of fig. 4 suggests a quite similar behavior as for τ. Again the asymptotic law works well very close to the transition while for larger distances of 10% and more, the numerical solution diverges markedly slower than the asymptotic law would suggest.

The structure of eqs. (2), (3) is the same as for the incoherent functions of the elastic hard-sphere system [17], including the factorization property for the dynamics around the plateau. However, the exponent parameter λ as well as glass form factor (f_q^s, cf. fig. 2) and the critical amplitude (h_q^s, cf. fig. 2) do depend on the coefficient of restitution. Hence we conclude that the dynamics is not universal with respect to dissipation.

Mean-squared displacement. – Experiments as well as simulations focus on the MSD which is defined by

$$\delta r^2(t) := \left[\int \mathrm{d}\Gamma w(\Gamma) \frac{1}{N} \sum_i (\vec{r}_i(t) - \vec{r}_i(0))^2 \right]$$

and can also be obtained from the expansion of $\phi_q^s(t) = 1 - q^2 \delta r^2(t) + \mathcal{O}(q^4)$ for small wave numbers. The equation of motion for the MSD in the granular case reads

$$\begin{aligned} &\partial_t \delta r^2(t) + \tfrac{1+\varepsilon}{2} \nu_E \delta r^2(t) \\ &+ v_0^2 \int_0^t \mathrm{d}t' m^{(0)}(t-t') \delta r^2(t') = 6 v_0^2 t \end{aligned} \tag{4a}$$

and the memory kernel within MCT is given by $m^{(0)}(t) = \lim_{q \to 0} q^2 m_q^s(t)$, and reads

$$m^{(0)}(t) = \frac{1+\varepsilon}{2} \frac{n}{6\pi^2} \int_0^\infty \mathrm{d}k\, k^4 S_k c_k^2 \phi_k(t) \phi_k^s(t). \tag{4b}$$

The behavior of the MSD at the respective critical points for several ε is shown in fig. 5. The effective Enskog damping coefficient $\nu_E(1+\varepsilon)/2$ decreases for smaller ε, and this lesser damping causes the MSD for $\varepsilon = 0$ to be slightly larger than that for $\varepsilon = 0.5$ and $\varepsilon = 1$ in the time window $-2 \leqslant \log_{10} t \leqslant -1$ after the ballistic regime. For macroscopic times the solutions reverse their order and finally reach their long-time limits $6r_c^2$ with the localization length being defined by

$$r_c^2 = \lim_{t \to \infty} \delta r^2(t)/6 = 1/\lim_{t \to \infty} m^{(0)}(t). \tag{5a}$$

Similarly to the glass form factors, for the MSD an asymptotic expansion can be performed with the result similar to eq. (2)

$$\delta r^2(t)/6 = r_c^2 - h_{\mathrm{MSD}} G_\sigma(t). \tag{5b}$$

Together with the critical,

$$\delta r^2(t)/6 = r_c^2 - h_{\mathrm{MSD}} (t/t_0)^{-a}, \tag{5c}$$

and the von-Schweidler law,

$$\delta r^2(t)/6 = r_c^2 + h_{\mathrm{MSD}} (t/\tau)^b, \tag{5d}$$

the analysis of the elastic hard-sphere systems in [17] carries over to the dissipative case. The evolution of r_c and h_{MSD} with ε are shown in the insets of figs. 5 and 6. In addition, the limited applicability of the asymptotic critical law due to large corrections to scaling applies to elastic as well as dissipative hard spheres [10].

It is seen in the inset of fig. 5 that r_c decreases with ε which is corresponding to a higher packing fraction at the glass transition (cf. inset of fig. 2). In the inset of fig. 5 we show r_c as a function of ε. Based on the explicit dependence of the memory kernel on ε one would predict r_c to decrease with ε, whereas the increase of the critical packing fraction with increasing dissipation would suggest the opposite effect. Hence the dependence is nontrivial

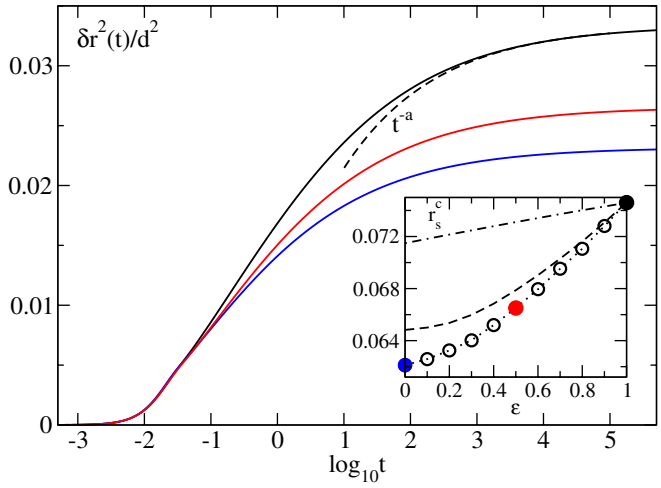

Fig. 5: (Colour on-line) Mean-squared displacement $\delta r^2(t)$ at the glass transition packing fraction $\varphi^c(\varepsilon)$ for coefficient of restitution $\varepsilon = 1.0$, 0.5, and 0.0 decreasing from top to bottom at long times. Full curves show the numerical solutions of eq. (4). The dashed curve displays the critical law in eq. (5c) with $t_0 = 0.035$ for the case $\varepsilon = 1.0$. The inset shows the localization length, cf. eq. (5a), as a function of ε with $\varepsilon = 1.0$, 0.5, and 0.0 shown as filled circles. The chain curve shows the elastic limit $r_c(\varepsilon = 1)$ scaled by the evolution of the mean particle separation, $\ell_0 \propto 1/(\varphi^c(\varepsilon)/\varphi^c(1))^{1/3}$. The dashed curve indicates the calculated localization length with the latter dependence scaled out.

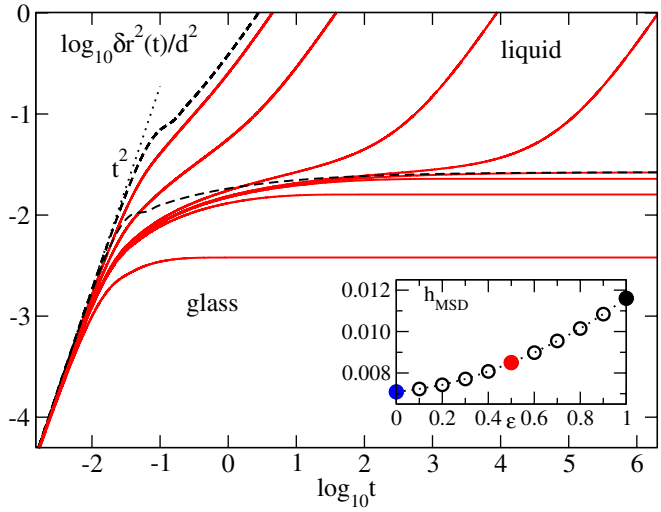

Fig. 6: (Colour on-line) Mean-squared displacement $\delta r^2(t)$ for coefficient of restitution $\varepsilon = 0.5$ and packing fractions $\varphi = \varphi^c$, $1.001\varphi^c$, $1.01\varphi^c$, $1.1\varphi^c$, on the arrested side —$0.999\varphi^c$, $0.99\varphi^c$, $0.9\varphi^c$, and 0.4, respectively, on the diffusive side. The terms liquid and glass indicate the diffusive and arrested regimes, respectively. Dashed curves show the results for the critical point and $\varphi = 0.4$ with the choice of $\nu_q = \nu_q^s = \nu_E = 0$. The initial ballistic law $v_0^2 t^2$ is shown by a dotted straight line. The inset exhibits the critical amplitude $h_{\rm MSD}$ as a function of ε.

and in fact we observe a decrease of r_c with increasing dissipation which is even stronger than the effect of the critical density alone.

While the overall decrease of r_c from $\varepsilon = 1$ to $\varepsilon = 0$ is more than 16%, the trivial contribution from the increase in density can explain only 4% of the decrease: A length scale can be defined by the inverse cubic root of the packing fraction which gives a scaling factor $(\varphi^c(\varepsilon)/\varphi^c(\varepsilon = 1))^{1/3}$. When the calculated results are scaled with this factor, the dashed curve in the inset of fig. 5 is found. Hence, the major part of the decrease of the localization length is a more involved prediction than just a simple density scaling argument.

Short-time dynamics. – It is known that the damping ν_q together with the early part of the memory kernel can overestimate the total damping considerably, which is an issue that cannot be fully resolved [8]. It is possible to estimate the order of magnitude of that effect without introducing mathematical inconsistencies by setting all the damping terms, ν_q, ν_q^s, ν_E to zero and solve the equations. The result is shown as the chain curve for $\phi_q^s(t)$ in fig. 1 for $\varepsilon = 0.5$ and $\varphi = 0.4$. Outside the transient regime, the undamped solution is shifted by 45% compared to the damped solution. For the MSD in fig. 6 for the same values of ε and φ, it results in a similar shift of 45% in time scales. At the transition point, however, the solutions with and without damping deviate from each other for the relatively large window $-2 < \log_{10} t < 1$, which is still outside the regime of applicability of the power law discussed above. It is also seen that the curves with Enskog damping deviate from the short-time asymptote $3v_0^2 t^2$ considerably earlier in time. Together, those effects can mask the glassy dynamics expected for moderately large windows in time that are accessible to experiments and simulation.

Summary and outlook. – In conclusion, the results discussed above and in [7] suggest for testing the theory experimentally. While for the variation of the packing fraction, φ, one expects to recover most features known from the thermal glass transition — from the variation of ε the following scenario should emerge:

1) The glass transition shifts to higher packing fractions φ^c for lower ε, cf. inset of fig. 2. Since the overall change is around 10% it should be measurable directly. The behavior of time scales and diffusion coefficient of the MSD demonstrated in fig. 4 supports the possibility of extracting this change from a dynamical experiment; even the asymptotic scaling law can be used reliably. In experiments on elastic systems, it is found that the critical density is shifted to higher values, $\varphi^c_{\rm exp} \approx 0.58$, as compared to the MCT prediction. Hence, also the transition for dissipative systems will be shifted to yet higher values of φ.

2) The localization length r_c decreases for the mean-squared displacement (cf. inset of fig. 5), and the corresponding plateau values f_q^s (cf. fig. 2) increase for smaller ε. While an absolute determination of f_q^s and r_c from measured $\delta r^2(t)$ and $\phi_q^s(t)$ may be ambiguous due to limited windows in time, a comparative measurement

between different ε should be within experimental resolution for the MSD, cf. fig. 5.

3) The α-scaling function for the long-time decay of the correlation functions and the MSD changes with ε. Since absolute changes in the critical exponents are comparably small, see inset of fig. 2, direct observation of changes in the exponents is probably rather difficult. However, a qualitative method is given by testing the α-scaling: For fixed ε, curves for different φ scale along their plateau value onto a single master curve, cf. figs. 1 and 3. In contrast, when going on a path along the transition in the ε direction, a violation of this α-scaling is expected.

While one can expect that the overall behavior of the MCT for granular systems is similar in two and three dimensions as is the case for the elastic hard-sphere system [19], the necessary glass form factors, critical amplitudes, and exponents cannot be estimated without performing the actual calculation. The dynamical scenarios observed in two dimensions [3,6] nevertheless support the existence of a glass transition in a driven granular fluid. In addition, a scenario for the evolution of $\phi_q^s(t)$ is found in [4] that is quite reminiscent of the 3D case shown in fig. 1. However, in contrast to the binary mixture in [3], the results from [4] have to be taken with some caution as the monodisperse experiment has a higher tendency towards ordering which may influence the observed dynamics. In all two-dimensional experiments, the estimated plateau of the MSD is around $4r_c^2 \approx 0.01d^2$, which is consistent with results anticipated from fig. 5. However, the values reported for the localization length in refs. [1,2] are smaller than predicted here by a factor of 10^3. One possible explanation for such a deviation is the influence of accelerations due to gravity [20] which might be remedied by future experiments under microgravity.

* * *

We thank DFG for funding under FG 1394.

REFERENCES

[1] Menon N. and Durian D. J., *Science*, **275** (1997) 1920.
[2] Goldman D. I. and Swinney H. L., *Phys. Rev. Lett.*, **96** (2006) 174302.
[3] Abate A. R. and Durian D. J., *Phys. Rev. E* , **74** (2006) 031308.
[4] Reis P. M., Ingale R. A. and Shattuck M.D., *Phys. Rev. Lett.*, **98** (2007) 188301.
[5] Fiege A., Aspelmeier T. and Zippelius A., *Phys. Rev. Lett.*, **102** (2009) 098001.
[6] Gholami I., Fiege A. and Zippelius A., *Phys. Rev. E*, **84** (2011) 031305.
[7] Kranz W. T., Sperl M. and Zippelius A., *Phys. Rev. Lett.*, **104** (2010) 225701.
[8] Götze W., *Complex Dynamics of Glass-Forming Liquids: A Mode-Coupling Theory* (Oxford University Press, Oxford) 2009.
[9] van Megen W., Mortensen T. C., Williams S. R. and Müller J., *Phys. Rev. E*, **58** (1998) 6073.
[10] Sperl M., *Phys. Rev. E*, **71** (2005) 060401.
[11] Brilliantov N., Poeschel T., Kranz T. and Zippelius A., *Phys. Rev. Lett.*, **98** (2007) 128001.
[12] Huthmann M. and Zippelius A., *Phys. Rev. E*, **56** (1997) R6275.
[13] Chong S.-H., Götze W. and Singh A. P., *Phys. Rev. E*, **63** (2001) 011206.
[14] Boon J.-P. and Yip S., *Molecular Hydrodynamics* (McGraw-Hill, New York) 1980.
[15] Franosch T., Fuchs M., Götze W., Mayr M. R. and Singh A. P., *Phys. Rev. E*, **55** (1997) 7153.
[16] Hansen J.-P. and McDonald I. R., *Theory of Simple Liquids*, 2nd edition (Academic, London) 1986.
[17] Fuchs M., Götze W. and Mayr M. R., *Phys. Rev. E*, **58** (1998) 3384.
[18] Fuchs M., *J. Non-Cryst. Solids*, **172-174** (1994) 241.
[19] Bayer M., Brader J., Ebert F., Lange E., Fuchs M., Maret G., Schilling R., Sperl M. and Wittmer J. P., *Phys. Rev. E*, **76** (2007) 011508.
[20] Durian D. J., *J. Phys.: Condens. Matter*, **12** (2000) A507.